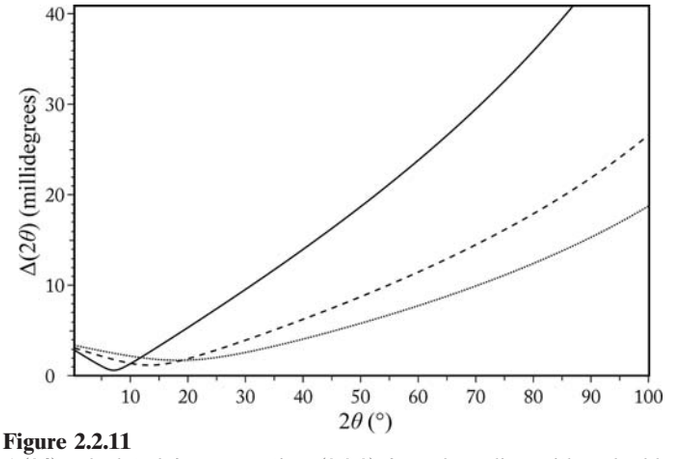

Figure 2.2.11
$\Delta(2\theta)$ calculated from equation (2.2.2) for a beamline with a double-crystal Si(111) monochromator, an Si(111) analyser ($\Delta_m = \Delta_a$ and $\theta_m = \theta_a$) and an FWHM vertical divergence of 25 μrad at λ = 0.4 Å (solid line: $\Delta_m \simeq 8.3$ μrad, $\theta_m = 3.6571°$), λ = 0.8 Å (dashed line: $\Delta_m \simeq 16.6$ μrad, $\theta_m = 7.3292°$) and λ = 1.2 Å (dotted line: $\Delta_m \simeq 25.2$ μrad, $\theta_m = 11.0319°$).

$$b = \tan\theta_a/\tan\theta_m - 2\tan\theta/\tan\theta_m.$$

Here α represents the vertical divergence from the source, δ is the difference between the Bragg angles of a central ray reflected from the monochromator at the angle θ_m and of another ray at angle θ'_m such that $\delta = \theta'_m - \theta_m$, and θ_a is the Bragg angle of the analyser crystal. The terms α'_m, Δ'_m and Δ'_a are related to the FWHM of the Gaussians representing the vertical divergence distribution or the Darwin widths of the monochromator and analyser crystals, α_m, Δ_m and Δ_a, respectively, with

$$\alpha'_m = \alpha_m/2(\ln 2)^{1/2}, \quad \Delta'_m = \Delta_m/2(\ln 2)^{1/2}, \quad \Delta'_a = \Delta_a/2(\ln 2)^{1/2}.$$

From the above equation, the intrinsic FWHM of the Gaussian-approximated peaks of the powder-diffraction pattern can be obtained as

$$\Delta^2(2\theta) = \alpha_m^2\left(\frac{\tan\theta_a}{\tan\theta_m} - 2\frac{\tan\theta}{\tan\theta_m} + 1\right)^2 + \tfrac{1}{2}\Delta_m^2\left(\frac{\tan\theta_a}{\tan\theta_m} - 2\frac{\tan\theta}{\tan\theta_m}\right) + \Delta_a^2. \quad (2.2.2)$$

Note that the true peak shape is not Gaussian, and a pseudo-Voigt (*e.g.* as described by Thompson *et al.*, 1987), Voigt (*e.g.* Langford, 1978; David & Matthewman, 1985; Balzar & Ledbetter, 1993) or other function modelled from first principles (*e.g.* Cheary & Coelho, 1992; Ida *et al.*, 2001, 2003) is usually better. Examples of FWHM curves calculated from equation (2.2.2) are plotted in Fig. 2.2.11 at three wavelengths. Differentiating the Bragg equation gives $\Delta d/d = -\cot\theta\,\Delta(\theta)$, where θ is in radians.

Gozzo *et al.* (2006) have extended the formulation of Sabine to include the effects of collimating and focusing mirrors in the overall scheme. Axial (horizontal) divergence of the beam between the sample and the detector causes shifts and broadening of the peaks, as well as the well known low-angle peak asymmetry due to the curvature of the Debye–Scherrer cones. Sabine (1987*b*), based on the work of Hewat (1975) and Hastings *et al.* (1984), suggests the magnitude of the broadening, $B(2\theta)$, due to horizontal divergence Φ can be estimated *via*

$$B(2\theta) = (\tfrac{1}{4}\Phi)^2(\cot 2\theta + \tan\theta_a),$$

where B and Φ are in radians. This value is added to $\Delta(2\theta)$.

2.2.4.1.2. *Hart–Parrish design*

A variant of the parallel-beam scheme replaces the analyser crystal with a set of long, fine Soller collimators (Parrish *et al.*, 1986; Parrish & Hart, 1987; Parrish, 1988; Cernik *et al.*, 1990; Collins *et al.*, 1992) (Fig. 2.2.12). The collimators define a true angle of diffraction, but with lower 2θ resolution than an analyser crystal because their acceptance angle is necessarily much larger and so the transmitted intensity is greater. They are not particularly suitable for fine capillary specimens, as the separation between foils may be similar to the capillary diameter, resulting in problems of shadowing of the diffracted beam. However, they are achromatic, and so do not need to be reoriented at each change of wavelength, which may have advantages when performing anomalous-scattering studies around an element's absorption edge. Unlike an analyser crystal, however, they do not suppress fluorescence. Peak shapes and resolution can be influenced by reflection of X-rays from the surface of the foils, or any imperfections in their manufacture, *e.g.* if the blades are not straight and flat. The theoretical resolution curve of such an instrument can be obtained from equation (2.2.2) by setting $\tan\theta_a$ to zero and replacing the angular acceptance of the analyser crystal Δ_a with the angular acceptance of the collimator Δ_c.

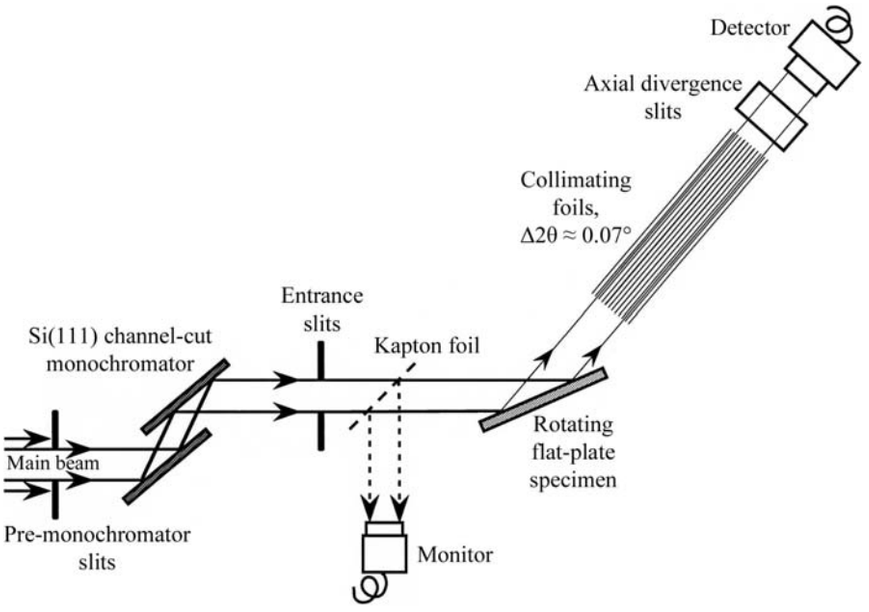

Figure 2.2.12
Schematic representation of a parallel-beam diffractometer of the Hart–Parrish design. The collimators installed on Stations 8.3 and 2.3 at the SRS Daresbury (Cernik *et al.*, 1990; Collins *et al.*, 1992) had steel blades 50 μm thick, 355 mm long, separated by 0.2 mm spacers, defining a theoretical opening angle (FWHM Δ_c) of 0.032° and a transmission of 80%.

2.2.4.2. *Debye–Scherrer instruments*

The simplest diffractometer has a receiving slit at a convenient distance from the sample in front of a point detector such as a scintillation counter. The height of the slit should match the capillary diameter, or incident beam height for flat plates. A slightly larger antiscatter slit near the sample should also be employed to reduce

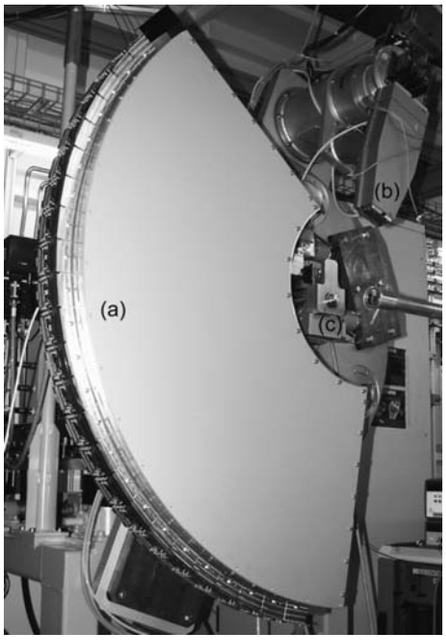

Figure 2.2.13
(*a*) 120° Mythen detector box, containing helium, mounted on the powder diffractometer of the materials science beamline at the Swiss Light Source. (*b*) Multianalyser detector stage. (*c*) Capillary spinner. (Bergamaschi *et al.*, 2009, 2010.)

background. The detector arm is scanned and a powder pattern recorded. This arrangement can be used for narrow capillary samples on lower-flux sources, avoiding the loss of intensity that use of an analyser crystal entails. The resolution is largely determined by the opening angle defined by the capillary and the receiving slit. Despite the simplicity of such an instrument, high-quality high-resolution data can be obtained.

For much faster data acquisition, a one-dimensional (1D) PSD or an area detector can be employed. Any sort of 1D detector with an appropriate number of channels, channel separation, efficiency, count rate (in an individual channel and overall) and speed of read out can be employed. Technology evolves and detectors make continual progress in performance. At the time of writing the most advanced 1D detector is the Mythen module developed by the Swiss Light Source (SLS). Mythen modules are based on semiconducting silicon technology and have 1280 8-mm-wide strips with a 50 μm pitch (64 × 8 mm^2). They can be combined to form very large curved detectors such as that on the powder diffractometer of the materials science beamline at the SLS (Fig. 2.2.13). This detector consists of 24 modules, 30 720 channels, set on a radius of 760 mm, covering 120° 2θ. Detector elements are therefore separated by ∼0.004°. The whole detector can be read out in 250 μs. Being Si based, its efficiency falls off above 20–25 keV, where the absorbing power of Si falls to very small values. Nevertheless, at intermediate and low energies a full powder-diffraction pattern for structural analysis can be measured in just seconds, or even faster if the intention is to follow a dynamic process.

Two-dimensional (2D) detectors are generally flat, so cannot extend to the same 2θ values as a curved multistrip detector unless scanned on a detector arm. This is possible, but usually a short wavelength is used with a fixed detector. This allows an adequate data range to be recorded, particularly if the detector is positioned with the direct beam ($2\theta = 0$) near an edge. A 2D detector records complete or partial Debye–Scherrer rings, which increases the counting efficiency with respect to scanning an analyser crystal by several orders of magnitude. In addition, if the rings do not appear smooth and homogeneous, this indicates problems with the sample, such as preferred orientation or granularity, both of which can seriously affect diffraction intensities when measuring just a thin vertical strip. Detectors that have been used are diverse and include image plates, though these have slow read out, charge-coupled devices (CCDs) or Si-based photon-counting pixel detectors used for single-crystal diffraction or protein crystallography (*e.g.* Broennimann *et al.*, 2006), and medical-imaging detectors, which are designed for hard-energy operation. Examples include the CCD-based Frelon camera, developed at the ESRF (Labiche *et al.*, 2007), and commercially available large flat-panel medical-imaging detectors up to 41 × 41 cm^2, based on scintillator-coated amorphous silicon, which have been exploited at speeds of up to 60 Hz for selected read-out areas (Chupas, Chapman & Lee, 2007; Lee, Aydiner *et al.*, 2008; Daniels & Drakopoulos, 2009).

Note that a 2D detector can be used as a 1D detector by applying a mask and reading out only a narrow strip, which can enhance the rate of data acquisition. For CCD chips, the electronic image can be rapidly transferred to pixels behind the masked part of the detector from where it can be read out while the active area is re-exposed. Translating an image plate behind a mask is a simple way of acquiring a series of diffraction patterns for following a process with modest time resolution.

These instruments are vulnerable to aberrations that cause systematic shifts in peak positions, such as misalignment of the capillary or surface of the sample from the diffractometer axis, and specimen transparency, which also affects the peak width and shape. The peak width also depends on whether a flat sample is in the $\theta/2\theta$ condition, or on the diameter of a capillary sample, *etc*. Focusing the incident beam onto the detector decreases the peak width, as fewer pixels are illuminated compared to using a highly collimated incident beam. PSDs are much more open detectors than those behind an analyser crystal or set of slits, so are more susceptible to background and parasitic scatter from sample environments *etc*. However, the speed and efficiency of data acquisition usually outweigh such concerns.

2.2.4.3. *Energy-dispersive instruments*

The broad, continuous spectrum from a wiggler or bending magnet is suitable for energy-dispersive diffraction (EDD). Here, the detector is fixed at an angle 2θ and the detector determines the energy, ε, of each arriving photon scattered by the sample (Fig. 2.2.14). The energy [keV] can be converted to d-spacing [Å] *via*

$$d \simeq 12.3984/2\varepsilon \sin\theta.$$

The detector usually consists of a cryogenically cooled semiconducting Ge diode. An absorbed X-ray photon promotes electrons to the conduction band in proportion to its energy. By

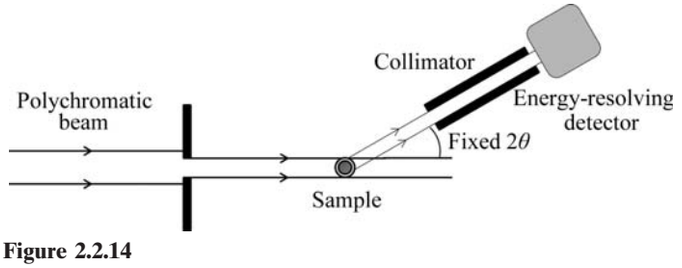

Figure 2.2.14
Schematic representation of an energy-dispersive diffraction arrangement.

references